Article ID: 1000-324X(2021)05-0541-06 **DOI:** 10.15541/jim20200286

$Zr_2Al_3C_4$ Coatings on Zirconium-alloy Substrates with Enhanced Adhesion and Diffusion Barriers by Al/Mo-C Interlayers

YE Wenhao[1,2], WEI Qiang[1,3], LIANG Jiamin[1,2], ZHOU Jie[2,4], MENG Fanping[2], EKLUND Per[4], HUANG Qing[2]

(1. School of Materials Science and Engineering, Tianjin University, Tianjin 300350, China; 2. Engineering Laboratory of Advanced Energy Materials, Ningbo Institute of Materials Technology and Engineering, Chinese Academy of Sciences, Ningbo 315201, China; 3. School of Mechanical Engineering, Hebei University of Technology, Tianjin 300130, China; 4. Thin Film Physics Division, Dept. of Physics, Chemistry, and Biology (IFM), Linköping University, Linköping 581 83, Sweden)

Abstract: Zircaloy coating is one of the crucial technical ways to improve the accident tolerance of nuclear fuel cladding, which enables the zirconium-water reaction problems to be solved. $Zr_2Al_3C_4$ coating is one type of candidate solutions to improve the high-temperature oxidation resistance of zirconium claddings. However, little study has been performed on the synthesis of $Zr_2Al_3C_4$ coatings on zirconium alloy substrates due to the inter-diffusion, as well as the difference of the thermal expansion coefficients between the $Zr_2Al_3C_4$ coating and the substrates. In this study, $Zr_2Al_3C_4$ coatings were prepared through room-temperature magnetron sputtering and post annealing on zirconium alloy (ZIRLO) substrates with magnetron-sputtered Al/Mo-C interlayers. The effects of Al/Mo-C interlayers on phases and microstructures of Zr-Al-C coatings after annealing were studied by different methods. It is found that the coatings without interlayer are broken and no $Zr_2Al_3C_4$ phase is formed due to significant interdiffusion between the Zr-Al-C coating and the substrate during annealing at 800 ℃ for 3 h. The Al/Mo-C interlayers prevented elemental diffusion between Zr-Al-C coatings and substrates during the post-annealing process. The Al/Mo-C interlayers act as diffusion barriers and greatly reduce the stoichiometric deviations from $Zr_2Al_3C_4$ phase, which facilitates the formation of the $Zr_2Al_3C_4$ phase in the final coating. Moreover, this diffusion-barrier layers contribute to eliminating cracks induced by the difference of the thermal expansion coefficients between the $Zr_2Al_3C_4$ coatings and substrates. At the same time, the adhesions between Zr-Al-C coatings with Al/Mo-C interlayers and substrates were improved after annealing, with their strength exceeding 30 N.

Key words: $Zr_2Al_3C_4$; coating interlayer; diffusion; adhesion

The 2011 Fukushima accident led to world-wide concern to increase the safety margin of light water reactors (LWRs) with respect to Zr-based cladding oxidation in high-temperature steam due to loss-of-coolant-accident (LOCA)[1-2]. One solution for accident-tolerant fuel is the development of oxidation-resistant coatings on Zr-based alloys to delay or eliminate the deleterious impact of LOCA[3-4].

The $M_{n+1}AX_n$ (MAX) phases, where M is an early transition metal, A is an A- group (primarily group 13 or 14) element, X is C or N, and n is an integer generally equal to 1, 2 or 3, have great potential applications as bulks and coatings because of their unique combination of the merits of ceramics and metals[5-7]. More recently, Zr-based MAX phases ($Zr_{n+1}AlC_n$) have attracted interest for the nuclear sector, because of the small thermal neutron-capture cross-section and high neutron economy exhibited by Zr[8]. In addition, Al offers the possibility of forming a protective Al_2O_3 layer in oxidative environments, and C is the preferred X-element as it avoids producing the long-lived ^{14}C radioisotope during irradiation[9]. More specifically, Zr-based MAX phases are considered

Received date: 2020-05-25; **Revised date:** 2020-08-20; **Published online:** 2020-10-30
Foundation item: National Natural Science Foundation of China (51873146); Ningbo Municipal Natural Science Foundation (2018A610005); Major Project of the Ministry of Science and Technology of China (2015ZX06004-001); Swedish Government Strategic Research Area in Materials Science on Functional Materials at Linköping University (Faculty Grant SFO-Mat-LiU No. 2009 00971)
Biography: YE Wenhao(1995–), female, Master candidate. E-mail: 1097706905@qq.com
叶文浩(1995–), 女, 硕士研究生. E-mail: 1097706905@qq.com
Corresponding author: WEI Qiang, professor. E-mail: weiqiang.tju@163.com; HUANG Qing, professor. E-mail: huangqing@nimte.ac.cn
魏 强, 教授. E-mail: weiqiang.tju@163.com; 黄 庆, 研究员. E-mail: huangqing@nimte.ac.cn

as candidate protective coatings designed to enhance accident tolerance of zirconium alloy for light water reactors. In the past three years, Zr_3AlC_2 and Zr_2AlC phases have been synthesized in bulk, but the materials still contain large amounts of ZrC phase[10-11]. Qarra, *et al.*[12] investigated the heavy ion irradiation damage in Zr_2AlC-rich material, and found that irradiated Zr_2AlC was partially amorphous at room temperature but remained crystalline at high temperature.

In the Zr-Al-C system, there is also a series of layered carbides based on the chemical formula $(ZrC)_nAl_3C_2$ or $(ZrC)_nAl_4C_3$ (where n=1, 2, 3…), such as $Zr_2Al_3C_4$ and $Zr_3Al_3C_5$[13]. These hexagonal phases with inherently nanolaminated crystal structures show similarities to traditional MAX phases. They can be described as ZrC_x in NaCl-type structure interleaved by Al_3C_2 or Al_4C_3 unit[14-15], and have better high-temperature mechanical properties and better compatibility with Zr-base cladding materials than typical MAX phases. For example, at 1400 ℃, the Young's moduli of the $Zr_2Al_3C_4$ and $Zr_3Al_3C_5$ ceramics are 331 and 319 GPa, respectively[16]. He, *et al.*[17] investigated the oxidation behavior of $Zr_2Al_3C_4$ at 1600 and 1750 ℃, and found that the formed scales are intact and strongly bonded with the substrate.

These ternary layered ceramics in the Zr-Al-C system are also investigated for possible use in nuclear reactors, but there are fewer studies on the synthesis of Zr-Al-C-based coatings to protect Zr-based alloy fuel clads, such as zircalloy and ZIRLO. It is difficult to deposit Zr-Al-C-based coatings on Zr alloys, including $Zr_2Al_3C_4$. Firstly, extensive inter-diffusion between the coating and the substrate leads to deviation from stoichiometry of the coating at high temperature, which can result in impurity phases. Secondly, the coefficients of thermal expansion (CTE) mismatch between the Zr-alloy substrate (~7.2×10^{-6} K^{-1}) and the Zr-Al-C coating (~8.1×10^{-6} K^{-1}) could affect adhesion[18]. In previous study, we preliminarily synthesized $Zr_2Al_3C_4$ coatings with Al-C/Si interlayers as diffusion barriers during the post-annealing, but the coatings were cracked by thermal stress[19].

In the present study, we used an Al/Mo-C interlayer structure, which can impede inter-diffusion between the coating and the substrate to help the formation of the $Zr_2Al_3C_4$ phase and improve the thermal-expansion matching to obtain an adherent and stable coating.

1 Experimental

The monolithic Zr-Al-C coating and the Al/Mo-C interlayer system were deposited on ZIRLO substrates at room temperature, by using magnetron sputtering system (KYZK Development Co, Ltd, China), and the design of the layered stacks was shown in Fig. 1. The nominal composition (wt%) of ZIRLO substrate is given as follows, Zr bal; Nb, 1.10; Sn, 1.10; O, 0.13; Fe, 0.11. The substrates were ultrasonically cleaned for 10 min in acetone then ethanol, and were blown dry in N_2. The vacuum chamber was evacuated to a base pressure of approximate 0.1 mPa. The DC magnetron power was set at 150, 42, 450, and 50 W for four targets of Zr_2Al, Al, graphite, and Mo, respectively. Prior to deposition, the targets were pre-sputtered for at least 15 min. During the deposition process, the working pressure of Ar was maintained at 0.5 Pa, with the substrate DC bias of –15 V. A shutter was installed between the target and the substrate holder to allow the deposition of one element. After deposition, the samples were isothermally annealed at 800 ℃ for 3 h in the vacuum below 2 mPa. The heating and cooling rates were both set at 5 K/min.

X-ray diffractometry (XRD) for phase identification was performed by a Bruker D8 Advance diffractometer with a Cu K_α radiation at a step of θ=0.02°. Surface and cross-section microstructures were examined by a field emission scanning electron microscope (SEM, FEI Quanta FEG 250). The compositional profiles of the coatings were determined by energy dispersive X-Ray spectroscopy (EDX, Oxford instruments X-MAX 50), with an accelerating voltage of 20 kV. Transmission electron microscope (TEM) characterization was performed in an FEI Tecnai F20 microscope operated at an acceleration voltage of 200 kV. The cross-sectional TEM samples were prepared by focused ion beam (FIB) microscope (Auriga, Carl Zeiss). Firstly, a target area of 5 μm ×7 μm was selected on the surface of the sample, and a layer of Pt (1–2 μm) is deposited on the target area to protect the sample. Then the rectangular region was bombarded to a depth of 5 μm by the Ga ion beams. The sides of the samples were thinned to 500 nm at the voltage of 30 kV and the current of 6–3 nA, and was further thinned to 100 nm when the voltage and current were reduced to 5 kV and 130 pA, respectively. Scratch tests were performed using a CSM Revetest scratch tester (CSM Instruments, Switzerland) with a Rockwell C diamond indenter with a

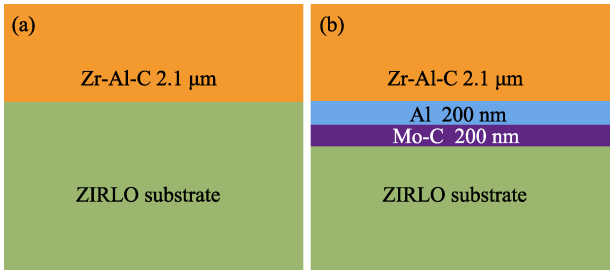

Fig. 1 Schematic views of the monolithic Zr-Al-C coating and the Al/Mo-C interlayer system

tip radius of 200 μm. The indenter was moved at the speed of 0.05 mm/s, and the linear loading rate was 1–50 N in 60 s.

2　Results and discussion

2.1　Zr-Al-C coatings without interlayer on ZIRLO substrates

The average atomic ratio of the deposited Zr-Al-C coatings is as follows: Zr 30.3%, Al 46.3%, C 23.4%. The results indicate that the composition of the films is close to the ideal stoichiometry of Zr:Al (2:3) in the $Zr_2Al_3C_4$ phase. SEM images of the surface and cross-section of the Zr-Al-C coatings on Zr-alloy substrate (as-deposited and annealed at 800 ℃) are shown in Fig. 2. It can be seen that the as-deposited coating is uniform and dense, but exhibit some small holes. The thickness of the coating is approximately 2.1 μm and the growth of the coating is columnar.

However, after annealing at 800 ℃ for 3 h, the coating shows a completely different morphology, being granular, and exhibiting other defects. As shown in Fig. 2(c), the coating shows a number of cracks; cracks are also observed for coatings annealed at other temperatures. The CTE mismatch between the substrate and the coating will induce cracking of the coating after annealing at high temperature. The cross-section SEM image in Fig. 2(d) shows that a reaction zone is formed between the coating and the substrate. The EDS line-scan also indicated that Al diffused into substrate and some Zr diffused into the coating. The Al and Zr compositions of the annealed coating by EDS are as follows: Al 16.8%, Zr 34.3%. The Al/Zr ration decreases to 0.49 after annealing. It can therefore be concluded that it is necessary for an interlayer both to improve the thermal expansion mismatch and consequently adhesion, and to prevent interdiffusion. Fig. 3 shows XRD patterns of the as-deposited and annealed coatings on the ZIRLO substrates without any interlayer.

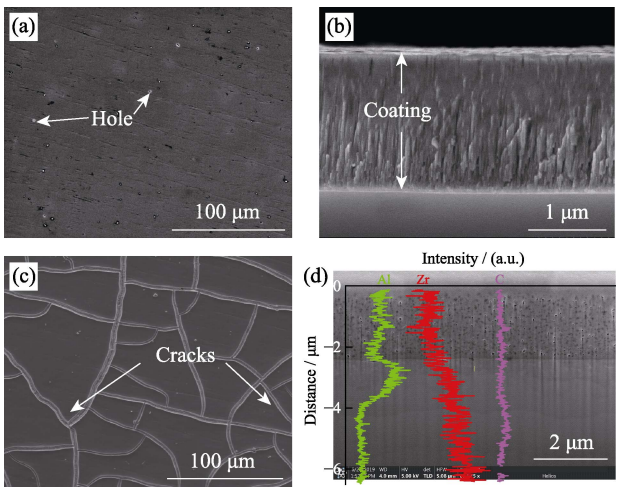

Fig. 2　SEM images of the monolithic Zr-Al-C coating on ZIRLO substrate

(a-b) Surface top view and cross section view of as-deposited coating; (c-d) Surface top view and cross section view of the coating annealed at 800 ℃ and its EDS line-scan

2.2　Zr-Al-C coatings with Al/Mo-C interlayer on ZIRLO substrates

Fig. 4 shows the SEM images of the surface and cross section of the 800 ℃-annealed coatings on ZIRLO substrates. In Fig. 4(a), the annealed coating is smooth, dense, uniform, and free of cracks, holes or other defects at this length scale. The as-synthesized $Zr_2Al_3C_4$ coating has an anisotropic microstructure of lath-like interlaced growth (Fig. 4(b)), which is consistent with the structure of the bulk $Zr_2Al_3C_4$ reported in the literature[15]. The cross-sectional image in Fig. 4(c) shows that the interface between the coating and the Al/Mo-C diffusion barrier layer is clear. A thin diffusion layer of approximate 200 nm thickness can be clearly observed between the Mo-C layer and the substrate. Fig. 4(d) shows the EDS line-scan profiles of this annealed coating cross-section from the surface to the substrate. The noticeable enrichment of Mo indicates hardly out-diffusion of the Mo element during annealing. In this study, the deposition time of the Zr-Al-C coating and the Al interlayer are 180 and 30 min, respectively, with the same power of Al target −42 W. So the Al-rich region locates in the Zr-Al-C coating instead of the intermediate pure Al layer. This result indicates that the interdiffusion between the substrate and the ternary layered ceramic coating should be negligible. The relative atomic concentrations of the Al and Zr elements at the surface coating are estimated to be 47.1% and 31.2%, respectively, which are close to the stoichiometry ratio of $Zr_2Al_3C_4$ phase.

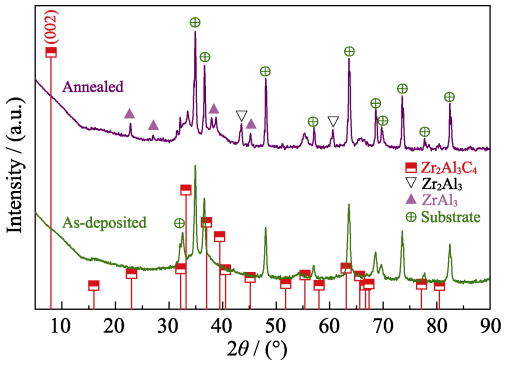

Fig. 3　XRD patterns of the as-deposited and annealed coatings on ZIRLO substrates without any interlayer

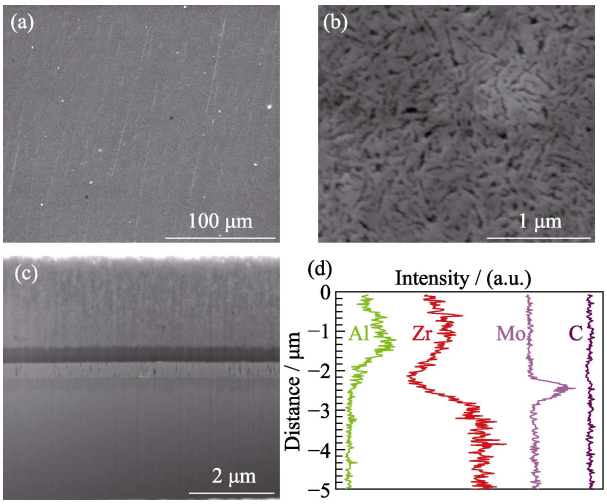

Fig. 4 SEM images of the multilayered C-Mo/Al/Zr-Al-C annealed coatings on ZIRLO substrate and EDS line scan along the cross-section

(a-b) Surface top view; (c) Cross section view; (d) EDS-line scan of the coating along the cross-section line in (c) from top and bottom

The XRD patterns of the as-deposited and annealed coatings with Al/Mo-C interlayer are shown in Fig. 5. The as-deposited multilayer coating exhibits similar diffraction peaks to the monolithic coating, but the annealed coating is completely different. The typical diffraction peak at 2θ=7.9° was detected in the XRD pattern, which can be assigned to diffraction from the basal planes (002) of the $Zr_2Al_3C_4$ phase. Furthermore, the seven peaks at 2θ=22.9°, 33.2°, 36.8°, 40.5°, 45.3°, 51.7°, 55.5° and 66.5° belonged to the $Zr_2Al_3C_4$ phase (PDF# 78-1801). After annealing at 800 ˚C for 3 h, the $Zr_2Al_3C_4$ phase formed in the coating with the C-Mo/Al interlayer, as demonstrated in the XRD pattern of the annealed coating. Besides the $Zr_2Al_3C_4$ phase, the $ZrAl_3$ and the $Zr_3Al_3C_5$ phases were also detected in the annealed coating. In the synthesis of $Zr_2Al_3C_4$ bulk, it was found that $Zr_2Al_3C_4$ balanced with ZrC, $Zr_3Al_3C_5$, and Zr-Al intermetallics[14]. As indicated in the phase diagram of Zr-Al-C at 700 ˚C, $Zr_2Al_3C_4$ is thermodynamically stable in the triangular zone with $Zr_2Al_3C_5$, $Zr_3Al_3C_5$ and $ZrAl_3$.

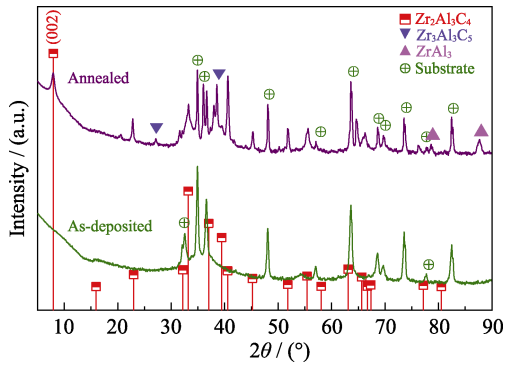

Fig. 5 XRD patterns of as-deposited and annealed coatings on ZIRLO substrates with Al/Mo-C interlayer

In order to get more information about the microstructures of the coatings before and after annealing, the as-deposited and annealed multilayer coatings were characterized by TEM. The cross-section bright field TEM images of as-deposited C-Mo/Al/Zr-Al-C multilayer coatings on ZIRLO substrates are shown in Fig. 6(a-c). In the low magnification image (Fig. 6(a)), a detail of this multilayer structure is clearly observed: it is clearly visible that the Zr-Al-C, and -Al with C-Mo as the initial layer deposited on the substrate are stacked in sequence. Fig. 6(b-c) show the selected-area electron diffraction pattern (SADE) and bright-field TEM image of the Zr-Al-C layer. The presence of the single halo ring indicates that the deposited layer has a typical amorphous structure. Fig. 6(d-f) show the cross-sectional TEM images of the composite coating annealed at 800 ˚C. As shown in Fig. 6(d), the interface of the interlayer can still be clearly observed after annealing. In Fig. 6(e), the selected area diffraction from the Zr-Al-C layer region consists of several diffractions and spots, indicating that the grain orientation is random. In a high-resolution TEM image (Fig. 6(f)), the typical nanolaminated microstructure similar to the traditional MAX phase is shown. The layered pattern has a vertical period of 2.22 nm, which matches with the *c* lattice parameter of $Zr_2Al_3C_4$[7,15].

2.3 Coating-substrate adhesion

Fig. 7(a) shows the images of the whole scratch track of the Zr-Al-C annealed coating without interlayer and its acoustic emission (AE) siginal as the function of load. It is also obvious from the optical micrograph that there are a large number of vertical and horizontal cracks on the surface of the coating. When the load initially increases from 0 N, the corresponding AE signal shows large fluctuations, indicating strong effects between the coating and the substrate. The coating begins to peel off partially from the substrate as the load increases, and the substrate is completely exposed at a normal load of ~ 9 N. In contrast, according to the scratch test, the adhesion of the multilayer coating substrate system is stronger than that of the monolithic layer. An image of the whole scratch track of the Zr-Al-C coating with C-Mo/Al interlayer and its AE signal as the function of load, are shown in Fig. 7(b). Besides some local delamination and fragment, the multilayer coating retained strong adhesion on the Zr substrate when the normal load varies from 0 to 30 N. The coating began to locally peel from the substrate at the normal load of 30 N, so the adhesion of the multilayer coating-substrate can be increased to 30 N. The thermal stress generated during heating could be effectively alleviated by the Al/Mo-C interlayer. In Fig. 4(c-d), mixed C, Mo and Zr could be observed in the diffusion zone of approximately 200 nm. The diffusion zone could also increase the adhesion of the coating.

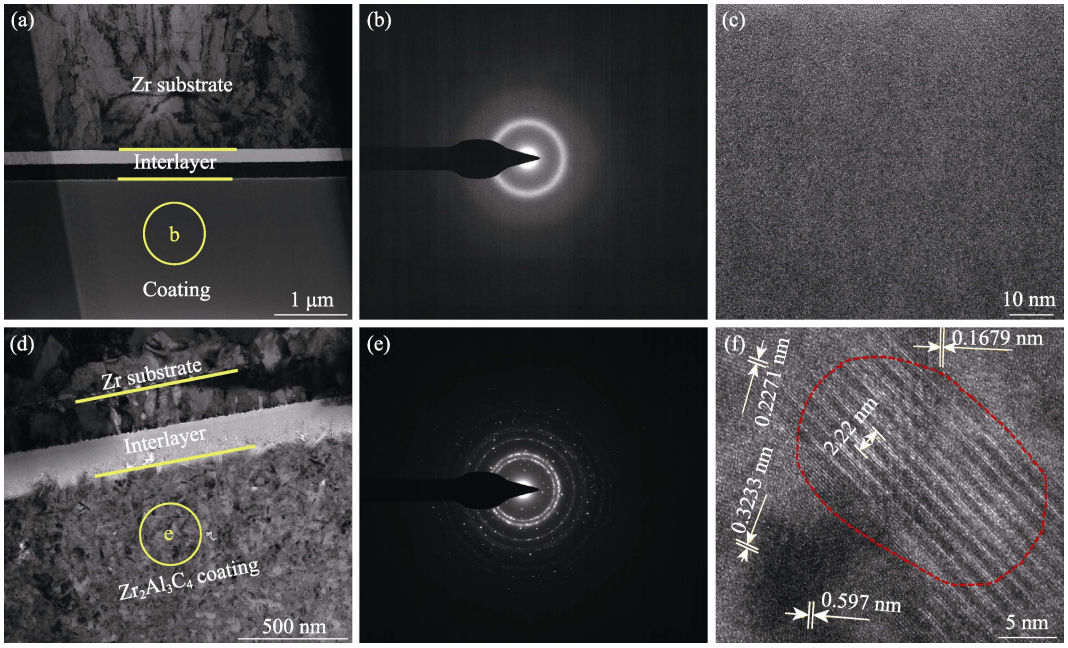

Fig. 6　TEM cross-section images and digital image of C-Mo/Al/Zr-Al-C multilayer coatings on ZIRLO substrates
(a, d) Overview images; (b, e) Selective area electron diffraction (SAED) patterns marked in (a) and (d), respectively; (c, f) HRTEM images

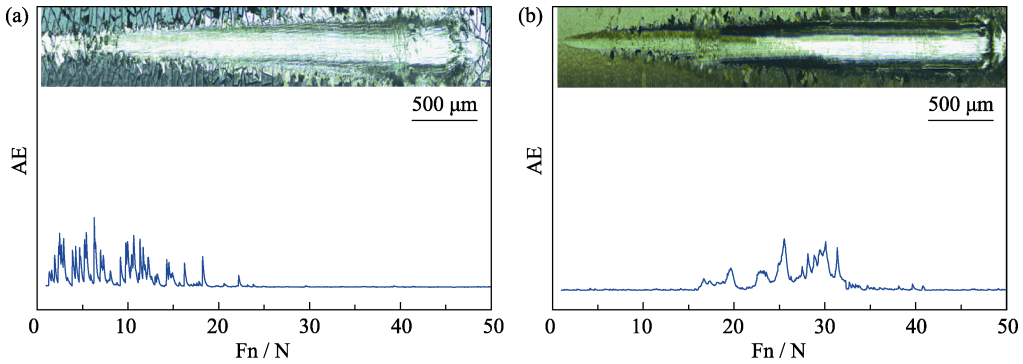

Fig. 7　Optical micrographs of scratch tracks and acoustic emission signals as functions of load for the annealed coatings on the Zr-substrate
(a) Zr-Al-C coating without interlayer; (b) Coating with Al/Mo-C interlayer

3　Conclusions

In summary, $Zr_2Al_3C_4$ phase was synthesized on ZIRLO substrates using magnetron-sputter-deposited Zr-Al-C coatings with Al/Mo-C interlayer post-annealed at 800 ℃ for 3 h. The interdiffusion between the Zr-Al-C coating and the ZIRLO substrate during annealing could be impeded by Al/Mo-C interlayer, which is helpful to form $Zr_2Al_3C_4$. At the same time, Al/Mo-C interlayer could alleviate the thermal stress of Zr-Al-C coating and the zirconium alloy substrate during the annealing to obtain a crack-free coating. Finally, the scratch test further confirmed that adhesion of the annealed Zr-Al-C coating-substrate was improved by the Al/Mo-C interlayer.

References:

[1] KIM H G, YANG J H, KIM W J, *et al.* Development status of accident-tolerant fuel for light water reactors in Korea. *Nuclear Engineering & Technology*, 2016, **48(1):** 1–15.

[2] PARK D J, KIM H G, JUNG Y I, *et al*. Behavior of an improved Zr fuel cladding with oxidation resistant coating under loss-of-coolant accident conditions. *Journal of Nuclear Materials*, 2016, **482(15):** 75–82.

[3] LEE C M, SOHN D S. Enhanced high-temperature oxidation resistance of a zircon-nium alloy cladding by high-temperature preformed oxide on the cladding. *Corrosion Science*, 2018, **131:** 116–125.

[4] KURATA M. Research and development methodology for practical use of accident tolerant fuel in light water reactors. *Nuclear Engineering & Technology*, 2016, **48(1):** 26–32.

[5] BARSOUM M W. The $M_{N+1}AX_N$ phases: a new class of solids: thermodynamically stable nanolaminates. *Progress in Solid State Chemstry*, 2000, **28(1):** 201–281.

[6] SUN Z M. Progress in research and development on MAX phase: a family of layered ternary compounds. *International Materials Reviews*, 2011, **56(3):** 143–166.

[7] LAI C C, TUCKER M D, EKLUND P, *et al*. Synthesis and characterization of $Zr_2Al_3C_4$ thin films. *Thin Solid Films*, 2015,

595: 142−147.
[8] HOFFMAN E N, VINSON D W, SINDELAR P L, *et al*. MAX phase carbides and nitrides: properties for future nuclearpower plant in-core applications and neutron transmutation analysis. *Nuclear Engineering and Design*, 2012, **244:** 17−24.
[9] THOMAS L, BENSU T, DANIEL P, *et al.* The double solid solution $(Zr, Nb)_2(Al, Sn)C$ MAX phase : a steric stability approach. *Scientific Reports*, 2018, **8(1):** 12801.
[10] LAPAUW T, LAMBRINOU K, CABIOC'H T, *et al*. Synthesis of the new MAX phase Zr_2AlC. *Journal of the European Ceramic Society*, 2016, **36:** 1847−1853.
[11] LAPAUW T, HALIM J, LU J, *et al*. Synthesis of the novel Zr_3AlC_2 MAX phase. *Journal of the European Ceramic Society*, 2016, **36:** 943−947.
[12] QARRA H H, KNOWLES K M, VICKERS M E, *et al*. Heavy ion irradiation damage in $Zr_3(Al_{0.9}Si_{0.1})C$ MAX phase. *Journal of Nuclear Materials*, 2020, **540.**
[13] ZHOU Y C, HE L F, LIN Z J, *et al*. Synthesis and structure–property relationships of a new family of layered carbides in Zr-Al(Si)-C and Hf-Al(Si)-C systems. *Journal of the European Ceramic Society*, 2013, **33(15/16):** 2831−2865.
[14] HE L F, LIN Z J, WANG J Y, *et al.* Synthesis and characterization of bulk $Zr_2Al_3C_4$ ceramic. *Journal of the American Ceramic Society*, 2007, **90(11):** 3687−3689.
[15] FUKUDA K, MORI S, HASHIMOTO S. Crystal structure of $Zr_2Al_3C_4$. *Journal of the American Ceramic Society*, 2005, **88(12):** 3528−3530.
[16] HE L F, LU X P, BAO Y W, *et al*. High-temperature internal friction, stiffness and strength of Zr-Al(Si)-C ceramics. *Scripta Materialia*, 2009, **61(1):** 60−63.
[17] HE L F, ZHONG H B, XU J J, *et al.* Ultrahigh temperature oxidation of $Zr_2Al_3C_4$ *via* rapid induction heating. *Scripta Materialia*, 2009, **60(7):** 547−550.
[18] PETUKHOV V. Thermal expansion of zirconium in the solid phase. *High Temperatures High Pressures*, 2003, **35-36(1):** 15−23.
[19] LIANG J M, WEI Q, GE F F, *et al.* Synthesis of $Zr_2Al_3C_4$ coatings on zirconium-alloy substrates with Al-C/Si interlayers as diffusion barriers. *Vacuum*, 2018, **160:** 128−132.

Al/Mo-C 中间层对锆合金表面 $Zr_2Al_3C_4$ 涂层界面性能影响

叶文浩[1,2], 魏 强[1,3], 梁佳敏[1,2], 周 洁[2,4], 孟凡平[2], EKLUND Per[4], 黄 庆[2]

(1. 天津大学 材料科学与工程学院, 天津 300350; 2. 中国科学院 宁波材料技术与工程研究所, 新能源技术研究所, 宁波 315201; 3. 河北工业大学 机械工程学院, 天津 300130; 4. Department of Physics, Chemistry, and Biology (IFM), Linköping University, Linköping 581 83, Sweden)

摘 要: 锆合金表面涂层研究作为提高核燃料包壳事故容错能力的重要技术手段之一, 能够有效解决失水事故下锆水反应的问题。$Zr_2Al_3C_4$ 以其优异的抗氧化性能和适用于核环境的化学组分而成为锆合金包壳的候选涂层材料之一。由于 $Zr_2Al_3C_4$ 涂层与锆合金基底之间的元素扩散以及热膨胀系数不匹配等问题, 在其上制备 $Zr_2Al_3C_4$ 涂层的相关研究较少。本研究通过磁控溅射结合后续热处理工艺, 以 Al/Mo-C 作为扩散屏障层, 在锆合金基底上制备 $Zr_2Al_3C_4$ 涂层。结合 X 射线衍射仪、扫描电子显微镜和透射电子显微镜等分析手段, 研究了 Al/Mo-C 中间层对涂层的相和微观结构的影响。结果表明, 在 800 ℃退火 3 h 后, 未添加中间层的涂层开裂, 同时由于 Zr-Al-C 涂层与基底之间存在明显的元素扩散, 导致 $Zr_2Al_3C_4$ 无法成相。Al/Mo-C 中间层作为扩散屏障, 能够有效阻止退火过程中 Zr-Al-C 涂层和基底之间的元素扩散, 从而大大降低 Zr-Al-C 涂层与标准化学量比的偏差, 有利于最终涂层中 $Zr_2Al_3C_4$ 相的形成。此外, 该扩散屏障层能够抑制 $Zr_2Al_3C_4$ 涂层在退火过程中产生裂纹, 同时将退火态涂层与锆合金基底的结合力提高 30 N。

关 键 词: $Zr_2Al_3C_4$; 中间层; 扩散屏障; 结合力

中图分类号: TB34 **文献标志码**: A